Origin of the Contact Angle Hysteresis of Water on Chemisorbed and Physisorbed Self-Assembled Monolayers

ARTICLE *in* LANGMUIR · SEPTEMBER 2012

Impact Factor: 4.46 · DOI: 10.1021/la3026717 · Source: PubMed

5 AUTHORS, INCLUDING:

Nataly Belman
Elbit Systems
18 PUBLICATIONS **359** CITATIONS
SEE PROFILE

Kejia Jin
Intralox LLC
14 PUBLICATIONS **125** CITATIONS
SEE PROFILE

Yuval Golan
Ben-Gurion University of the Negev
126 PUBLICATIONS **2,580** CITATIONS
SEE PROFILE

Jacob Israelachvili
University of California, Santa Barbara
282 PUBLICATIONS **19,572** CITATIONS
SEE PROFILE

Langmuir

Article

pubs.acs.org/Langmuir

Origin of the Contact Angle Hysteresis of Water on Chemisorbed and Physisorbed Self-Assembled Monolayers

Nataly Belman,[†] Kejia Jin,[‡] Yuval Golan,[§] Jacob N. Israelachvili,[†] and Noshir S. Pesika*[,‡]

[†]Department of Chemical Engineering, and Materials Department, University of California, Santa Barbara, Santa Barbara, California 93106, United States

[‡]Department of Chemical Engineering and Biomolecular Engineering, Tulane University, New Orleans, Louisiana 70118, United States

[§]Department of Materials Engineering and the Ilse Katz Institte for Nanoscale Science and Technology, Ben-Gurion University of the Negev, Beer-Sheva 84105, Israel

Supporting Information

ABSTRACT: Self-assembled monolayers (SAMs) are known to form on a variety of substrates either via chemisorption (i.e., through chemical interactions such as a covalent bond) or physisorption (i.e., through physical interactions such as van der Waals forces or "ionic" bonds). We have studied the behavior and effects of water on the structures and surface energies of both chemisorbed octadecanethiol and physisorbed octadecylamine SAMs on GaAs using a number of complementary techniques including "dynamic" contact angle measurements (with important time and rate-dependent effects), AFM, and electron microscopy. We conclude that both molecular overturning and submolecular structural changes occur over different time scales when such SAMs are exposed to water. These results provide new insights into the time-dependent interactions between surfaces and colloids functionalized with SAMs when synthesized in or exposed to high humidity or bulk water or wetted by water. The study has implications for a wide array of phenomena and applications such as adhesion, friction/lubrication and wear (tribology), surfactant–solid surface interactions, the organization of surfactant-coated nanoparticles, etc.

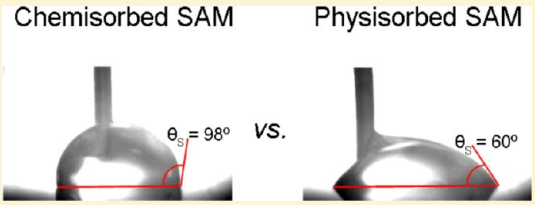

INTRODUCTION

Contact angle hysteresis is a widespread phenomenon that reflects nonequilibrium adhesion interactions involving liquids, that is, closely related to wetting, adsorption, and thin film phenomena and ultimately also to friction and lubrication forces of solid surfaces. Hysteresis theories generally invoke "physical" roughness, either intrinsic (static) or induced by the wetting liquid, but many very rough surfaces show little hysteresis.[1] Hysteresis due to "chemical" changes, e.g., in the hydrophilic–lipophilic balance (HLB), has been less considered, although already in 1937 Langmuir suggested "overturning" of physisorbed surfactants.[2] Such effects have been observed directly by the Israelachvili group[3] and the Klein group[4] and recently been proposed as the cause for the increased adhesion of geckos (whose toe surfaces are composed of β-keratin protein) in humid environments.[5] Such molecular overturning, submolecular reorientations, and related effects would affect the interfacial and surface energies γ_{SL} and γ_{SV} of advancing and receding liquid boundaries, i.e., three-phase contact lines, even at perfectly smooth surfaces.[6−9]

Thus, there are still no generally accepted theories of contact angle hysteresis, either based on surface roughness or changes in the various surface and interfacial energies, that can (quantitatively) predict γ_{SL} and γ_{SV} and/or slow dynamic effects, such as creep, or the phenomenon of stick–slip motion of a contact lines. On the experimental side, even the question of the equilibrium contact angle when different angles are measured on advancing (θ_A) and receding (θ_R) has still not been satisfactorily resolved. However, the Tadmor group, by considering the line energy contribution to the Young equation, derived an expression relating advancing and receding contact angles to the equilibrium contact angle, which has been validated for certain systems.[10]

Here we approach the problem experimentally, focusing on how the contact angles of advancing and receding droplets are determined by the three surface energies of the Young equation:[11]

$$\gamma_{SV} = \gamma_{LV} \cos\theta + \gamma_{SL} \quad (1)$$

Our system is the molecularly smooth single crystal surface of gallium arsenide (GaAs) modified with self-assembled monolayers of either physisorbed octadecylamine (ODA, $C_{18}H_{37}NH_2$) or chemisorbed octadecanethiol (ODT, $C_{18}H_{37}SH$). The surfaces were characterized using a number of complementary techniques, including contact angle measurements, optical microscopy, scanning electron microscopy (SEM), and atomic force microscopy (AFM).

Received: July 3, 2012
Revised: September 13, 2012
Published: September 14, 2012

dx.doi.org/10.1021/la3026717 | Langmuir 2012, 28, 14609−14617

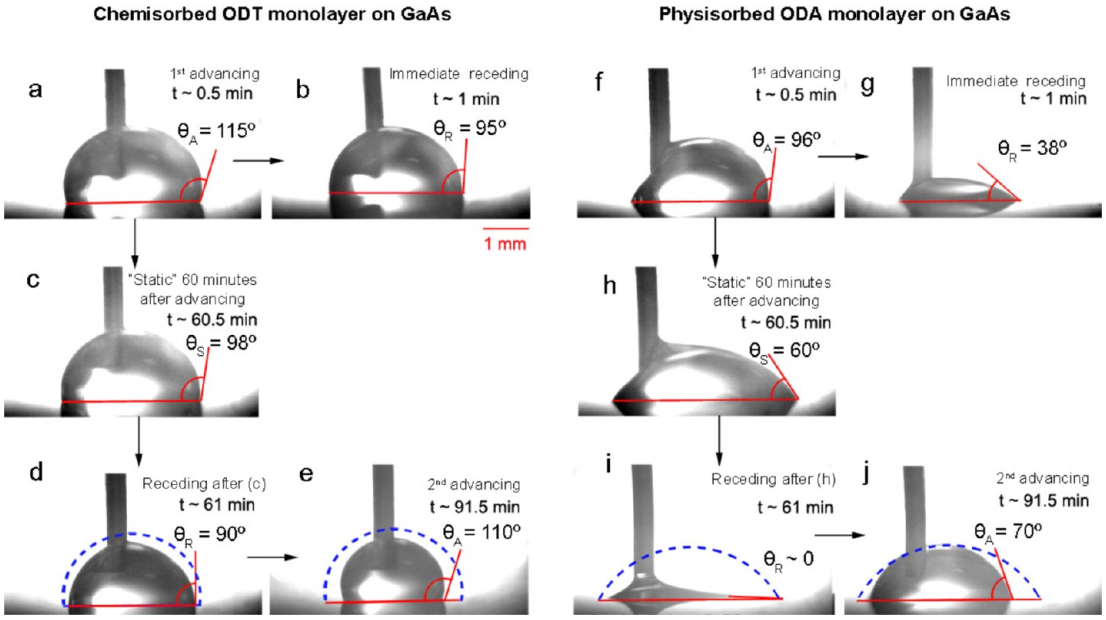

Figure 1. Side-view optical images of water drops on smooth GaAs surfaces modified with ODT or ODA SAMs. (a, f) Advancing drops (first advance), (b, g) receding drops immediately after advancing, (c, h) "static" drops 60 min after an advancing step, (d, i) receding drops after steps c and h, (e, j) advancing drops after drying the surfaces after steps d and i (second advance). The injection/suction rates were fixed at $\nu' = 1$ mL/h = 0.28 mm^3/s, which corresponded to advancing/receding rates of ~0.02 mm/s. θ_A, θ_R, and θ_S denote the advancing, receding, and "static" contact angles, respectively. "$t = 0$" is the time that an advance was initiated.

Although the primary aim of the study is to explore the origin of contact angle hysteresis on physisorbed and chemisorbed self-assembled monolayers, the practical implications of the study include gaining insights into the time-dependent interactions between surfaces and colloids functionalized with either chemisorbed or physisorbed SAMs when synthesized in, or exposed to, high humidity or bulk water which is important in adhesion,[12−14] friction, lubrication and wear (tribology),[15] the organization of surfactant-coated nanoparticles,[16,17] etc.

EXPERIMENTAL SECTION

Formation of Self-Assembled Monolayers (ODT and ODA SAMs). ODT (Aldrich, 98%) and ODA (Aldrich, 99%) were stored under argon at all times and used as received. Ethanol (200 Proof, Gold Shield), chloroform (HPLC grade, 99+%, Aldrich), and ammonium hydroxide (NH_4OH, ACS grade, 28−30%, EMD Chemicals) were used for all experiments. Deionized water (resistivity >18.2 MΩ cm) was obtained from a Millipore Milli-Q Integral 5 filter system. Single crystal polished GaAs wafers were undoped, with three orientations (111)A (i.e., Ga-terminated), (111)B (i.e., As-terminated), and (110) (i.e., mixed-face) (Wafer Technology Limited).

We chose to study in detail the As-terminated GaAs (111) face, since AFM measurements showed the smallest root-mean-square (rms) roughnesses on this surface of 0.58 ± 0.18 nm for ODT and 0.14 ± 0.05 nm for ODA SAMs as shown in Figure S1. In addition, the advancing contact angle θ_A was the highest on this surface (data on the other surfaces not shown), implying better organization of the SAMs on this face, and in agreement with results reported by McGuiness et al.[18]

GaAs wafers were cut into ~1.5 cm × 1.5 cm squares. The surfaces were then modified with either ODT or ODA SAMs following a modified protocol based on McGuiness et al.:[19] the GaAs wafers were immersed in concentrated NH_4OH for 10 min during which the native surface oxide layer was etched away. To form an ODT-modified GaAs surface ("ODT-SAM"), the oxide-free wafers were immediately immersed in a 2 mM ethanoic solution of ODT and kept in solution for 20 h under an Ar atmosphere. The wafers were then removed from the solution and sonicated in pure ethanol for 10 min to remove unbound ODT and then removed and dried with N_2. To form an ODA-modified GaAs surface ("ODA-SAM"), the wafers were removed from NH_4OH, rinsed with water, dried with N_2, and immediately placed into the 10 mM ODA solution in chloroform and kept in solution for 20 h under an Ar atmosphere. The wafers were then removed from the solution and gently rinsed with chloroform to remove any unbound ODA. The SAM-coated wafers were stored in a desiccator, under vacuum, before characterization.

Characterizations of the Self-Assembled Monolayers. Contact angle measurements were performed using a custom-built contact angle goniometer. A sealed contact angle cell was built of glass, steel, and Teflon. A syringe needle was manipulated from the outside by a motorized syringe device (Model 33, Harvard Apparatus). The advancing and receding contact angles were measured by increasing and reducing the drop volume at a constant volumetric flow rate. An external video camera was used to record the silhouette of the drop as a function of time. In certain cases, the drop formed on one side of the needle (as opposed to symmetrically around the tip of the needle) and the camera had to be repositioned to capture the entire drop silhouette. The humidity was maintained at ~85% by placing vials with water inside the chamber. All experiments were performed at 22 °C.

Pure water drops were used for the contact angle measurements. Very similar results were obtained with ODT or ODA-saturated water drops (since ODT and ODA are insoluble in water).[20] To obtain ODT/ODA-saturated solutions, a 1 mM ODT/ODA aqueous solution was sonicated for 10 min, stirred for 3 h, left overnight, and filtered using a 0.45 μm Teflon filter.

AFM imaging was carried out under ambient conditions using an Asylum MFP-3D instrument, operating in tapping mode, using silicon probes. Scan sizes were 1 × 1 and 25 × 25 μm^2, imaged at scan rates of 1 and 0.5 Hz, respectively.

For SEM imaging, the surfaces were examined with an FEI XL40 Sirion FEG digital scanning microscope.

RESULTS AND DISCUSSION

Figure 1 shows side-view images of dynamic contact angle measurements performed at constant flow rates of $\nu' = 1$ mL/h, which corresponds to an initial advancing/receding rate of the three-phase boundary of ~0.02 mm/s. The first advancing

dx.doi.org/10.1021/la3026717 | Langmuir 2012, 28, 14609−14617

contact angles θ_A were measured at the three-phase lines as shown in Figures 1a and 1f for the ODT- and ODA-SAMs, respectively. As soon as the drops attained a volume of 10 ± 2 μL (radius ∼1.5 mm), the water was either (1) immediately withdrawn (Figures 1b,g) to obtain the "immediate" receding contact angle θ_R or (2) the motorized syringe was turned off for t = 60 min (the "stopping time" or "resting time") to allow the system to approach equilibrium (Figures 1c,h). We refer to these angles as the "static" angles (even though they are not the "equilibrium" values: as discussed below, they are generally higher than after stopping for a similar time after a receding step).

We may note that the first advancing angles were always lower for the physisorbed ODA-SAMs than for the chemisorbed ODT-SAMs (compare Figures 1a and 1f). Also, for both SAMs, following an immediate reversal, the receding angles were always less than the advancing angles, but again the decrease was much more pronounced for the ODA-SAMs than the ODT-SAMs (cf. Figures 1b and 1g).

Even more dramatic differences were observed after the 60 min stopping times following the first advance, when the water was withdrawn at the same rate as the receding contact angle, θ_R, was recorded. The receding contact angles on the physisorbed ODA surfaces were now too small to measure, effectively zero (Figure 1i), and the three phase boundary remained pinned at the contact line. In contrast, the ODT receding angles (Figure 1d), while the lowest measured on the ODT-SAMs, were still very high (∼90°).

After the first receding steps (Figures 1d and 1i), in order to evaluate the changes in the SAMs due to the their long exposure to bulk water, the surfaces were fully dried, and 30 min later the second advancing angles were measured over the same areas as the first. For the ODT-SAMs, the second advancing contact angles were very similar to the first (cf. Figures 1e and 1a), but for the ODA-SAMs, the second advancing angles were always significantly lower than the first (cf. Figures 1j and 1f), again inferring large changes in the structure of the physisorbed ODA-SAMs.

All of these time effects, with respect to both the contact angles and the different interfacial and surface energy changes, are illustrated graphically later in Figures 2−4.

The differences in the contact angles between ODT-SAMs and ODA-SAMs on GaAs point to complex dynamic changes, reversible as well as irreversible, that occur within the monolayers, including monolayer reorganization upon advancing and receding, and even under "static" conditions (when exposed to water). Our data also show that the hysteresis cannot be attributed to static surface roughness, but rather to dynamic changes occurring in γ_{SL} and γ_{SV} in eq 1 when wetted by bulk water or (saturated) water vapor from the nearby bulk water surface of the droplet (for reasons already given, large changes in γ_{LV} can be discounted). Additional results, discussed below, provide further insight into the differences between physisorbed and chemisorbed SAMs and, ultimately, the subtle changes that explain the origin of the contact angle hysteresis on smooth SAM-modified surfaces.

As a reference, advancing angles on native GaAs were in the range θ_A = 54°−76°, increasing with the exposure time to the (ambient) atmosphere, and are attributed to the formation of a partially hydrophobic oxide layer which is removed (slowly dissolves) when the surface is immersed in water[21] and potentially from absorbed organic molecules from the air.[22] Removal of the oxide layer by etching with concentrated ammonia resulted in lower contact angles of θ_A = 50° and θ_R = 8°, which correspond to an equilibrium contact angle θ_{eq} ∼ 29° (calculated based on ref 10) and are somewhat higher than previously reported values of θ_{eq} ∼ 20° from the literature.[23] Literature values for the surface and interfacial energies of hydrocarbon (alkane)−water (bulk or vapor) combination are given in Table 1.

Table 1. Interfacial Energies of the Various Interfaces Involved in This Study at 22 °C[24,25]

interface	γ_i (mN/m or mJ/m^2)	comments
hydrocarbon−vapor, γ_{SV}	18.5	mainly CH_3 (e.g., pentane), close-packed monolayer
	27.5	mainly CH_2 (e.g., hexadecane)
hydrocarbon−water, γ_{SL}	50[a]	mainly CH_3, close-packed monolayer
	54[a]	mainly CH_2
water−vapor, γ_{LV}	72.5[b]	pure water; no surface-active agents in solution (≪ cmc)[b]

[a]The hydrocarbon−water interfacial tensions increase from about 50 to 54 mJ/m^2 on going from heptane to hexadecane,[24,25] which has been attributed to the increasing fraction of methylene $-CH_2$ groups and decreasing fraction of methyl $-CH_3$ groups on the molecules. [b]This condition was established to be valid in these experiments.

Figure 2 shows the changes that occur in the various "static" contact angles as a function of the "stopping time" or "resting time" after stopping the injection or suction of liquid, i.e., at constant droplet volume. Figure 2a shows the large differences in both the magnitudes and the hysteresis of chemisorbed ODT-SAMs (upper shaded region) and ODA-SAMs (lower region). Thus, in the case of the ODT-SAM, at the end of the first advance, the contact angle is ∼118° and gradually decreases to ∼100° after 60 min. The same drop was then receded, and "static" contact angle data were collected over a period of another 60 min. After the first receding step, the contact angle is ∼88° and then gradually increases to ∼92° after 60 min. Presumably, these two limiting contact angles are gradually approaching the (same) thermodynamic equilibrium value, θ_{eq}, which may safely be put between 88° and 92°; in other words, θ_{eq} = 90 ± 2°.

In the case of the ODA-SAM, the initial angle at the end of the first advance is also high (∼98°) but drops rapidly with the stopping time, to a value of ∼60° after 60 min, and upon receding, the contact line remained pinned (i.e., θ_R ∼ 0°) for the entire duration of the experiment.

These dynamic changes in the contact angles show (1) that molecular and chemical[21] processes (changes) occur within the SAMs and/or the GaAs surface both on advancing and receding, as well as after stopping after an advancing or receding step, and (2) that these changes are quite different (and much greater) for physisorbed (ODA) versus chemisorbed (ODT) SAMs, as well as equilibrating over different time scales (data presented later). And in contrast to the chemisorbed monolayer, no clear "thermodynamically equilibrium angle" could be established for the physisorbed monolayer (we return to consider and discuss this effect later).

On the basis of the measured contact angles, θ_S, in Figure 2a, we now attempt to establish what these molecular-level changes are by investigating which of the two surface and/or interfacial energies γ_{SL} and γ_{SV} are changing, on both advancing and receding. The changes in γ_{SL} or γ_{SV} were calculated using

dx.doi.org/10.1021/la3026717 | Langmuir 2012, 28, 14609−14617

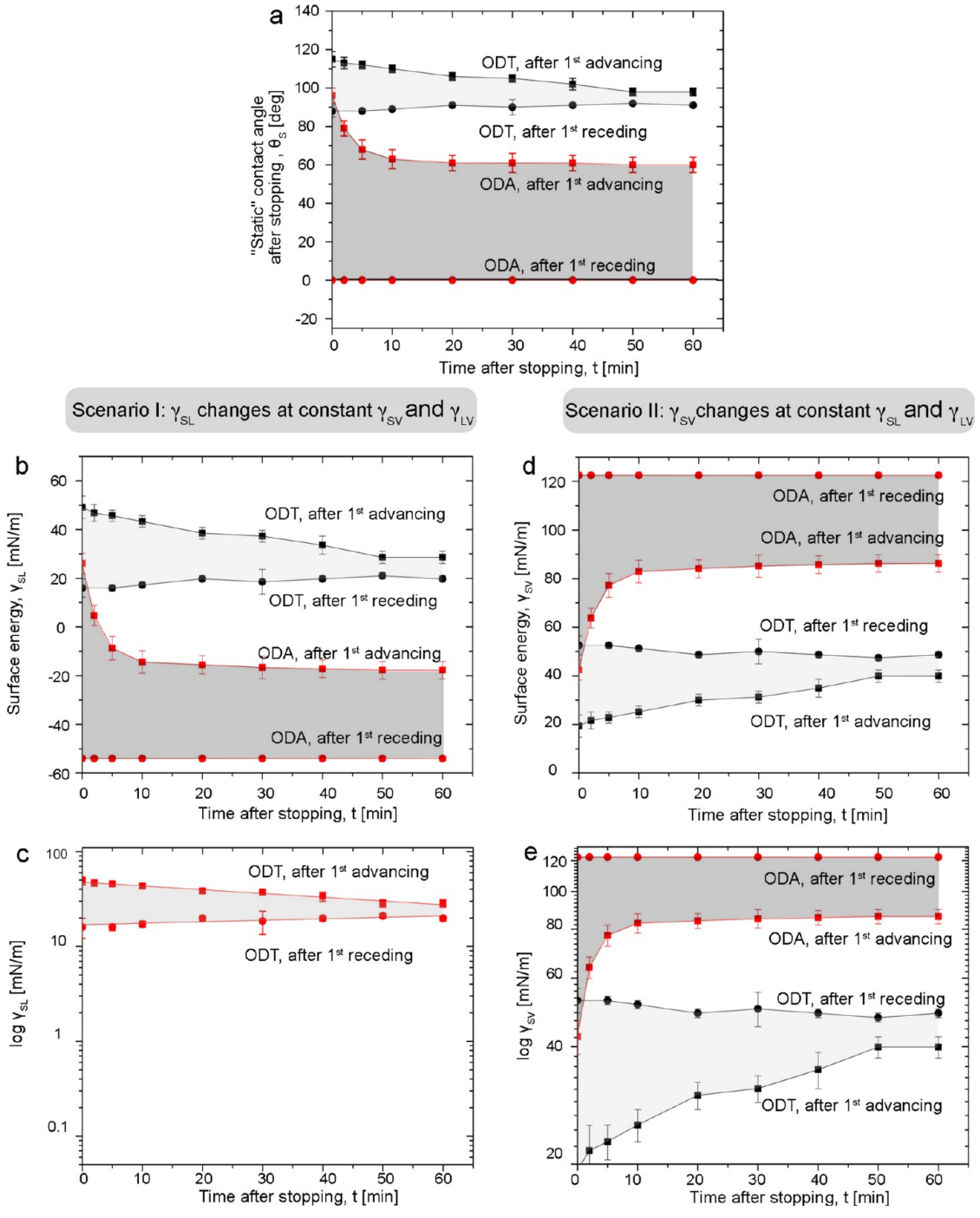

Figure 2. Time evolution of the "static" contact angles θ_S (defined when $v' = 0$, not when θ is not changing) on ODT- and ODA-SAMs of 10 ± 2 μL water drops vs the times, t, after stopping the advancing or receding. The droplets were advanced/receded at $v' = 1$ mL/h in either direction for ~30 s before stopping, which defines $t = 0$ in both cases. The first receding contact angle measurements were obtained from the same drop which was used to collect the first advancing contact angle measurements; therefore, $t = 0$ for the first receding contact angle measurement corresponds to $t \sim 1$ h (of bulk water exposure at the solid–liquid interface). (a) Contact angles θ_S vs stopping times, t (see images in the middle and lower rows of Figure 1). (b–e) The corresponding interfacial and surface energies γ_{SL} and γ_{SV}, plotted on both linear and log plots. (b, c) Scenario I: linear and log plots of the changes of the interfacial energies γ_{SL} vs t, calculated using eq 1 putting $\theta = \theta_S$ and assuming (see Table 1) that $\gamma_{SV} = 18.5$ mJ/m^2 and $\gamma_{LV} = 72.5$ mJ/m^2 remain constant. (d, e) Scenario II: linear and log plots of the changes of the interfacial energies γ_{SV} vs t, calculated using eq 1 putting $\theta = \theta_S$ and assuming (see Table 1) that $\gamma_{SL} = 50.0$ mJ/m^2 and $\gamma_{LV} = 72.5$ mJ/m^2 remain constant.

Young's equation (eq 1). In these calculations, the surface tension (energy) of the water/air surface was set to $\gamma_{LV} = 72.5$ mJ/m^2 (see Table 1), since in the case of the ODT-SAMs, the ODT molecules were covalently bound to the surface, while in the case of the ODA-SAMs, although ODA molecules could (and we later conclude that some did) desorb, the surface tension of the water/air interface is not expected to change significantly even in the case of complete desorption of the monolayer from the solid/liquid interface into the bulk solution (droplet reservoir).[26]

In the analysis and interpretation of the contact angle data of Figure 2a, it quickly becomes apparent that, even with the

dx.doi.org/10.1021/la3026717 | Langmuir 2012, 28, 14609–14617

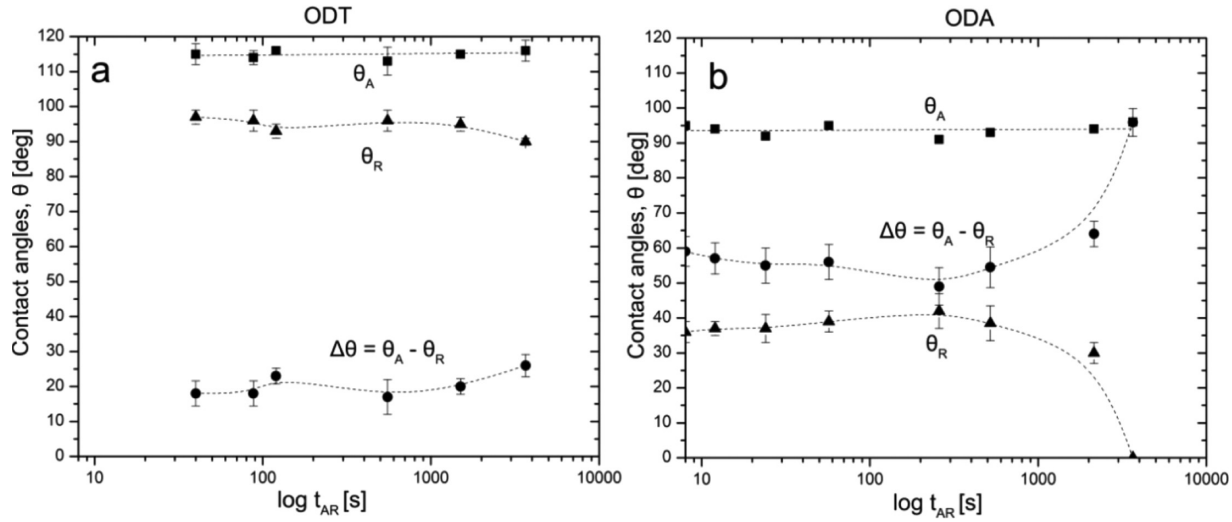

Figure 3. "Dynamic" or "slipping" first advancing and first receding contact angles as a function of the "total contact time" t_{AR} the monolayers were in contact with water (before the contact lines started to move) on (a) chemisorbed ODT-SAMs and (b) physisorbed ODA-SAMs. Also shown is the corresponding contact angle hysteresis, $\Delta\theta = (\theta_A - \theta_R)$. The measurements were made at injection/suction rates ranging from $v' = 0.03$ to 10 mL/h, corresponding to advancing–receding rates of 8.3×10^{-3}–0.2 mm/s, with no significant effects on the results (measured dynamic angles).

assumption that γ_{LV} is constant, there are two possible limiting scenarios as well as a combination of the two (e.g., with less strongly bound chemisorbed layers, where both mechanisms could be operating, presumably at different time scales): In scenario I, the interfacial tension of the monolayer–air (solid/vapor) interface γ_{SV} remains constant (see Table 1) at γ_{SV} = 18.5 mJ/m^2 (in addition to the water–vapor tension γ_{LV} = 72.5 mJ/m^2 remaining constant). This leads to Figures 2b,c for the interfacial tension of the monolayer–water (solid/liquid) interface, γ_{SL}. In scenario II, the interfacial tension of the monolayer–water (solid/liquid) interface γ_{SL} remains constant at γ_{SL} = 50 mJ/m^2 (see Table 1). This leads to Figures 2d,e for the interfacial tension of the monolayer–air (solid/vapor) interface, γ_{SV}.

In scenario I (Figures 2b,c), assuming constant γ_{SV} the time evolution of γ_{SL} for the ODT-SAM after the first receding step would imply that γ_{SL} close to the three-phase contact region increases from ∼15 to ∼20 mJ/m^2; i.e., the monolayer–water interface becomes *less hydrophilic* (or more hydrophobic) during the 60+ min the solid–liquid interface has been exposed to bulk water. This is highly improbable, and in the absence of a more physically plausible explanation, this scenario is tentatively discounted.

Alternatively, scenario II (Figure 2d,e) assuming constant γ_{SL} would imply that for the ODT-SAM after the first receding step the monolayer–vapor interfacial tension γ_{SV} close to the three-phase contact region decreases from ∼52 to ∼50 mJ/m^2. This can be readily explained by the gradual evaporation of water molecules from the previously fully wetted monolayer (which, even after being withdrawn from the bulk water phase, is still nanoscopically close to it, i.e., essentially exposed to saturated water vapor). Likewise, the increase in γ_{SV} from ∼20 to ∼40 mJ/m^2 after the first advancing step can be explained by the saturation of the vapor close to the three-phase contact region due to the proximity of the water droplet. Thus, from Figure 2d the thermodynamically equilibrium value of γ_{SV} for a chemisorbed ODT-SAM exposed to saturated water vapor or very close to a bulk water phase appears to be $\gamma_{SV} = 45 \pm 5$ mJ/m^2, which is higher than the value of ∼20 mN/m for a monolayer exposed to dry inert vapor (or vacuum).

Similar analyses can be made with the ODA-SAMs, but now we find that scenario I predicts negative values for γ_{SL} (Figure 2b), while scenario II predicts unphysically high values for γ_{SV} (Figure 2d). To make sense of these results, we first present some more data on (1) how the advancing and receding contact angles depended on the time the monolayers were exposed to water before the direction was reverse; for example, Figures 1g,i show that for ODA-SAMs the receding angle is θ_R ∼ 38° when the stopping time after an advance, before receding, is ∼1 min, but θ_R ∼ 0° when the stopping time is 60 min, and (2) how reversible and reproducible were the measurements after multiple back-and-forth advancings and recedings.

Figure 3 shows how the advancing and receding angles, and the contact angle hysteresis, $\Delta\theta = (\theta_A - \theta_R)$, varied with the total time t_{AR} that the SAMs were exposed to the (bulk) water droplet before the contact line started to move (t_{AR} varied between 0.1 and 60 min). For both SAMs, the advancing angles θ_A did not vary, i.e., were roughly constant, with the contact time t_{AR}, although the ODA-SAM had a significantly lower θ_A than the ODT-SAM.

Regarding the receding angles, for the ODT-SAMs (Figure 3a), θ_R showed a small but gradual decrease with the contact time, from ∼97° to ∼90°, inferring that (small) changes were occurring within the ODT-SAM over relatively large time scales. For the ODT-SAMs the contact angle hysteresis, $\Delta\theta = (\theta_A - \theta_R)$, was always small.

In contrast, for the ODA-SAMs (Figure 3b), θ_R showed a gradual increase and then a precipitous decrease with the contact time, reaching ∼0° after about 1 h of contact with bulk water. We may conclude that either the physisorbed monolayer had fully overturned, exposing a fully hydrophilic surface of amine groups, or the molecules had completely desorbed from the surface into the bulk water phase. For the ODA-SAMs the contact angle hysteresis, $\Delta\theta = (\theta_A - \theta_R)$, started at a low value, similar to ODT, but ended up at an extremely high value.

An additional effect that was noticed with ODA, but not with ODT-SAMs, was "stick–slip" motion of receding contact angles; this was manifested by a pinning (sticking) of the contact line as the drop volume was decreased on receding,

dx.doi.org/10.1021/la3026717 | *Langmuir* 2012, 28, 14609–14617

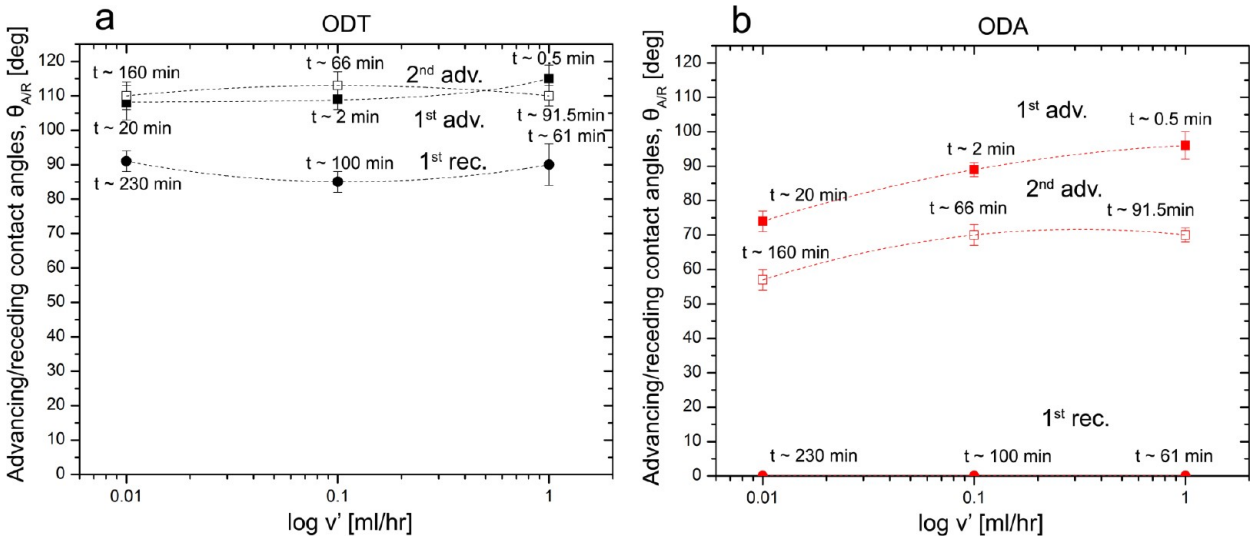

Figure 4. Dynamic advancing and receding contact angles of pure water droplets on (a) ODT-SAMs and (b) ODA-SAMs at constant volumetric flow rates of $v' = 1$, 0.1, and 0.01 mL/h, corresponding to front velocities of 2×10^{-2}, 2×10^{-3}, and 2×10^{-4} mm/s and advancing/receding times of ~40 s, 4 min, and 40 min, respectively, from start to finish, where $t = 0$ is the time of the first advance (slip). After the first advancing and first receding steps (at $t_{AR} = 60$ min), the surfaces were the left to dry until the droplet completely evaporated (~30 min) after which a new (second) advancing contact angle was measured over the same area as the first.

resulting in a decrease of the contact angle to say at $\theta_{pinned} \approx 30°$, until suddenly the edge moves forward (slips), leading to a sudden increase in the receding angle to, say, $\theta_R \approx 38°$ (see Figure 3b, which shows the slipping angles, not the pinned angles, θ_{pinned}). Such stick–slip behavior has previously been observed by Lam et al.[27] For $t_{AR} = 60$ min, the surface is perfectly wetted by the water droplet, with the contact line "permanently" pinned at the edge, resulting in $\theta_R = \theta_{pinned} \approx 0°$ (Figure 1i). The pinning at 0° suggests, and the subsequent finite second θ_A (Figure 4) confirms, that the water-exposed surface is not clean, bare GaAs, but contains some surfactant molecules, although, as discussed below, not as much as the original close-packed layer.

The effects of advancing/receding rates, v', on the contact angles on ODT- and ODA-SAMs were measured at three different volumetric injection/suction rates v' and are summarized in Figure 4. Rate effects were negligible for the chemisorbed ODT-SAMs (Figure 4a), but significant for the ODA-SAMs (Figure 4b), where higher rates led to higher advancing contact angles θ_A, ranging from $\theta_A \approx 74°$ at the lowest to $\theta_A \approx 95°$ at the highest advancing rates, which varied over a factor of ~100. Dynamic contact angles can be rate-dependent if inertial forces contribute, which can occur if the capillary number $Ca = \mu V/\gamma_{LV}$ is $>10^{-5}$,[28] where μ is the fluid viscosity, V the velocity of the moving contact line, and γ_{LV} the surface tension. For the droplets in these experiments Ca ranged from $\sim 10^{-9}$ to $\sim 10^{-7}$. We may therefore conclude that the observed rate dependence of θ_A on the ODA-SAMs cannot be attributed to inertial effects.

To further investigate the changes in the SAM-modified surfaces on exposure to water, after the first receding step the freshly exposed surfaces were left to dry until the droplets had completely evaporated (about 30 min), and a new droplet was then advanced again over the same area as the first (see Figures 1e,j and the second advancing steps in Figure 4). The second θ_A was the same as the first for the ODT-SAM, but was ~25% smaller for the ODA-SAM, again indicating that a change had occurred in the structure of the physisorbed SAM at the solid/liquid interface.

Figure 5 shows SEM and AFM images of the surfaces before and after the water droplets were advanced and receded from the surfaces. As seen from the AFM images in Figures 5a,b, continuous ODT and ODA monolayers are formed (as opposed to SAM patches). The SEM images in Figures 5c,d and magnified AFM images in Figures 5b,e,f show visual evidence for significant changes due to desorption on ODA-SAMs, while on the chemisorbed ODT-SAMs (Figure 5a) the changes or traces remaining from the drops or the boundaries could be barely distinguished by both SEM and AFM (not shown). On an ODA-SAM surface, the drop boundary (red arrows in Figure 5c) shows evidence of the pinning effect discussed above and loss of ODA molecules from the surface at the three-phase contact line. The width of the boundary was found to increase with contact time (data not shown). The dark gray area (marked as area 1 in Figures 5c,d) inside the boundary is the area where the drop receded. The middle circle of ~2 mm (area 2) is the point where the receding drop remained pinned. The inner circle of ~0.8 mm (area 3) is the concentrated area that was created due to the final drying up of the remainder of the drop.

The AFM scans performed at different areas of the drop are shown in Figures 5e,f. As can be seen, ODA molecules can rearrange to form islands on the surface, and in the more concentrated areas, the islands are denser and larger. The measured island height was 4.0 ± 0.5 nm in both cases (compare to the smoother native ODA-SAM surface in Figure 5b), very close to the value (4.5 nm) of the lamellar c-spacing of the orthorhombic ODA unit cell.[29,30] Similar dendritic flower-shaped domains have been observed by others on dioctadecylamine Langmuir monolayers at the air–water interface[31,32] where, in this case, the ODA islands were formed by desorbed molecules from the 3-phase contact line due to the unbalanced normal (tensile) component of γ_{LV} at the air–water interface, followed by their reassembly after the water droplet had completely evaporated.

dx.doi.org/10.1021/la3026717 | Langmuir 2012, 28, 14609–14617

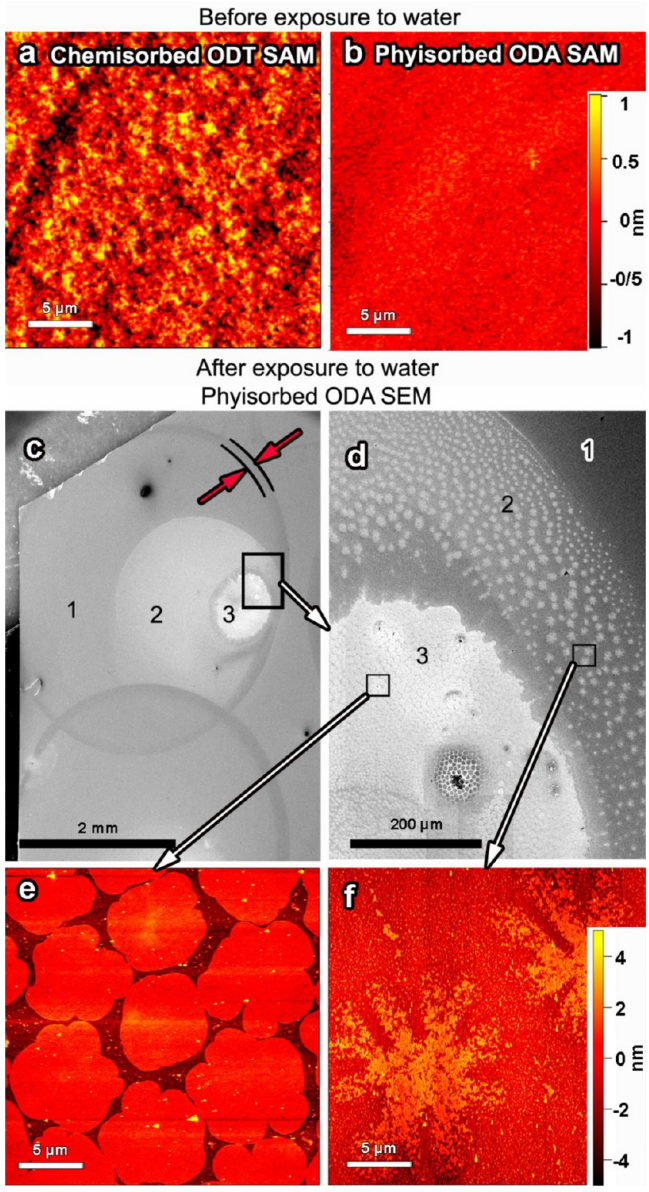

Figure 5. (a, b) AFM images of chemisorbed ODT-SAM and physisorbed ODA-SAM on GaAs prior to exposure to water. Note the rougher chemisorbed monolayer, due to the forced incommensurability induced by the covalent bonds with the GaAs lattice, in contrast to the stress-free "van der Waals epitaxial" ordering of the physisorbed monolayer. (c, d) SEM and (e, f) AFM images of an ODA-SAM after the advancing and receding steps of a water drop. Time t_{AR} = 4 min in this case (advancing rate v' = 1 mL/h, the receding rate v' = 0.3 mL/h). The drop was allowed to dry completely in the contact angle instrument chamber. The drop boundary is shown by red arrows in (c). The three different areas of the drop trace, marked as 1, 2, 3 in (c) and (d) are discussed in the text.

On the basis of the observations and measurements carried out on chemisorbed ODT and physisorbed ODA-SAMs on GaAs surfaces, and their analysis in terms of the Young equation, eq 1, discussed above, we present two schematics (Figures 6 and 7) that illustrate proposed mechanisms that appear to explain the contact angle hysteresis as well as the microscopic visualizations. The interfacial energies of the different regions at the first moment that liquid water contacts the surfaces are shown by the solid lines. The blue lines represent the interfacial energies on exposure to an advancing droplet; these profile would depend critically on the rate of advance as well as other factors, such as the droplet volume. For the ODT-SAMs (Figure 6), the blue line reveals an increase in γ_{SV} near the droplet surface (from 18.5 mN/m for a fully hydrophobic monolayer exposed to dry air). This is attributed to the high water content (essentially saturate vapor) in the vapor phase close to the 3-phase contact line as well as some water penetration into region I from the bulk liquid water region II. As the drop advances, the region closest to the contact line (i.e., region II) has had the least exposure time to bulk water, and therefore γ_{SL} is not expected to be affected significantly. However, region III has had more time to equilibrate with the bulk water, presumably involving water penetration into the SAM, which results in a lower γ_{SL}. Thus, upon receding after an advance, the contact line is exposed to two entirely different surfaces: one with a lower γ_{SL} and the other with a higher γ_{SV}, which gives rise to the contact angle hysteresis, where again the magnitude of $\Delta\theta$ may depend on both the advancing and receding rates as well as the "stopping" (resting or static) time between the end of the advance and the beginning of the receding.

A similar mechanism (Figure 7) is proposed to explain the origin of the contact angle hysteresis of water on ODA-SAMs with the added complexity of molecular overturning (regions III and IV) and desorption (regions V and VI). The small hump in γ_{SL} within region V corresponds to a transient state (see hump in the θ_R curve of Figure 3 at t around 200−300 s) of increased hydrophobicity. Figure 7 illustrates that this is what would be expected in the transition from the two quasi-hydrophilic regions IV to VI during which the hydrocarbon chains of the monolayers are once again exposed to the water right before desorption. In region VI, the monolayer has completely desorbed, exposing the hydrophilic substrate to the water, but the low γ_{SL} in this region does not rule out the existence of a dilute submonolayer of ODA molecules. A negative value of γ_{SL}, which is predicted by the Young equation, implies repelling (hydrophilic) surfaces that, thermodynamically, will eventually result in the dissolution of the substrate when exposed to water for a long time; i.e., it may be simply a reflection of a long-lived but metastable surface or interface that, energetically, "wants to dissolve away".

The results may be modeled by a recently proposed equation for the effective interfacial tension of a partially hydrophobic surface:[33] $\gamma_{SL} = \gamma_i(1 - a_0/a)$, where γ_i is the interfacial tension of the pure hydrocarbon−water interface, a is the exposed area per (surfactant) molecule, and a_0 is the molecular area in the unstressed monolayer or bilayer that exhibits no hydrophobic interaction. In future work, we plan to fit the experimental contact angle data from the chemisorbed and physisorbed SAM-modified GaAs surfaces with a recently proposed equation for hydrophobic interactions.[33]

CONCLUSIONS

A series of dynamic (advancing/receding) and rate-dependent contact angle measurements were performed on chemisorbed ODT-modified and physisorbed ODA-modified on single crystal GaAs surfaces to understand the origin of contact angle hysteresis on SAM-modified surfaces, which are molecularly smooth and where the (dynamic) hysteresis cannot (and could not) be attributed to (static) roughness effects. Contact angle hysteresis was much more prevalent on physisorbed ODA-modified GaAs surfaces compared to chemisorbed ODT-modified GaAs surfaces (even though the

dx.doi.org/10.1021/la3026717 | Langmuir 2012, 28, 14609−14617

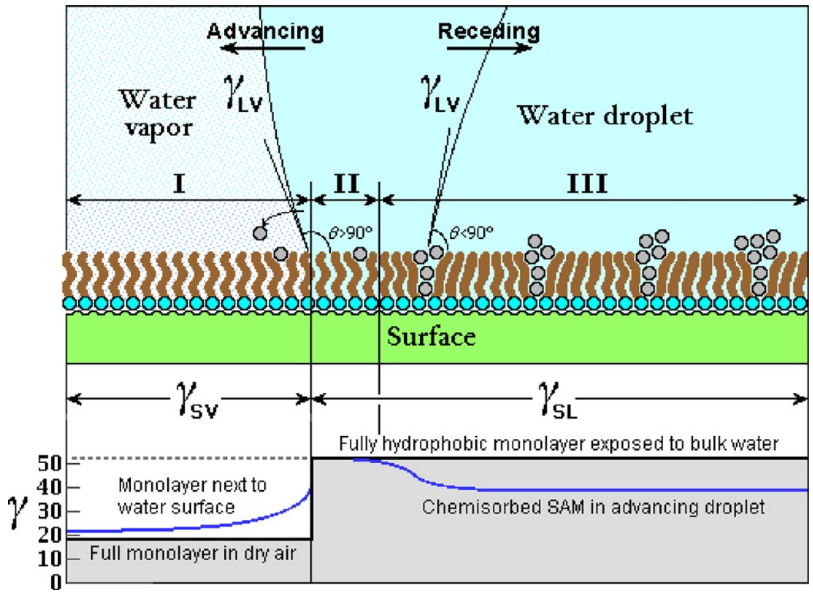

Figure 6. Schematic of proposed processes that lead to the contact angle hysteresis of chemisorbed SAMs. Region I: fully hydrophobic monolayer, but with water penetration near the contact line, especially on receding, which increases γ_{SV} (blue line) above the value of ~18.5 mN/m in dry air (solid line). Region II: fully hydrophobic monolayer with progressive penetration of water with time, which decreases γ_{SL} (blue line) below the value of ~50 mN/m for a fully hydrophobic monolayer in water (with no water penetration). Region III: partially hydrophobic monolayer in equilibrium with bulk water.

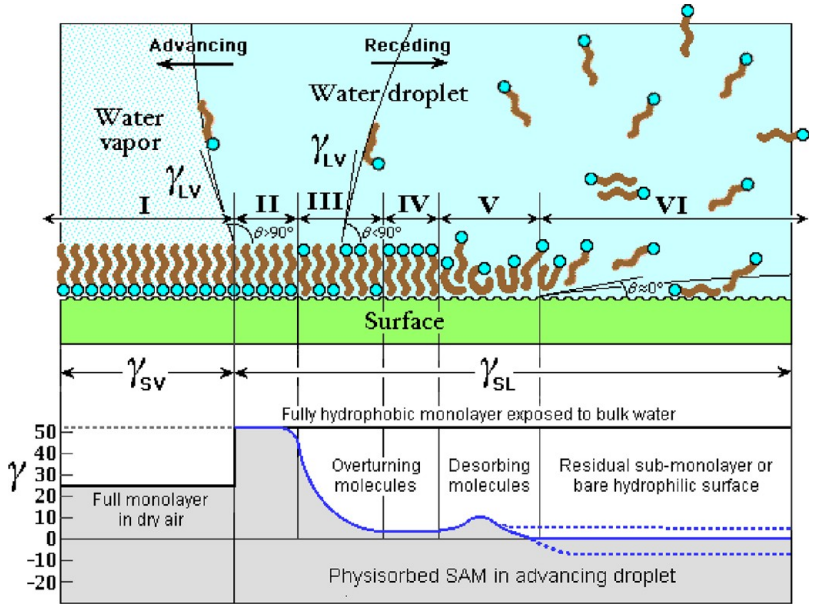

Figure 7. Schematic of proposed processes that lead to the contact angle hysteresis of physisorbed SAMs. Regions I–VI are described in the figure and in the text. In contrast to chemisorbed monolayers (cf. Figure 6) where the blue line represents the ultimately stable profile for the surface and interfacial energies, for physisorbed monolayers as we have here, the profile shown reflects the situation after a certain (finite) time, and continues to change as more molecules overturn and desorb from the surface.

latter was initially much rougher at the nanoscale) and is attributed to time-dependent rearrangements, overturning, and desorption effects that occur with physisorbed (ODA) molecules, while chemisorbed (ODT) molecules do not desorb from the solid/liquid interface and remain more or less intact when exposed to bulk water phase. Our results demonstrate that although surface roughness may be a factor contributing to contact angle hysteresis, in the SAM systems studied here, molecular rearrangements play the dominant role. These results also provide insights into the dynamic (rate- and time-dependent) interactions that can arise between physisorbed and chemisorbed SAMs surfaces or colloidal particles when exposed to bulk water or humidity.

■ ASSOCIATED CONTENT

Supporting Information

AFM images of ODT- and ODA-modified GaAs unique faces; XPS spectra of unique GaAs surfaces modified with a SAM of ODT; table of advancing and receding contact angles on unique GaAs surfaces modified with ODA- and ODT-SAMs.

dx.doi.org/10.1021/la3026717 | *Langmuir* 2012, 28, 14609–14617

This material is available free of charge via the Internet at http://pubs.acs.org.

AUTHOR INFORMATION

Corresponding Author

*E-mail: npesika@tulane.edu.

Notes

The authors declare no competing financial interest.

ACKNOWLEDGMENTS

We thank Tom Mates for the help with the XPS measurements. This work was supported by the US−Israel Binational Science Foundation, Grant 2006032 (J.N.I., Y.G.), NSF Grants CHE-1059108 (J.N.I., N.B.) and CBET-1034175 (N.P.), and DOE Grant DE-FG02-87ER-45331 (J.N.I., for the experimental design and interpretation of the results). This work made use of MRL Central Facilities supported by the MRSEC Program of the National Science Foundation under Award DMR05-20415.

REFERENCES

(1) Koch, K.; Bhushan, B.; Jung, Y. C.; Barthlott, W. Fabrication of Artificial Lotus Leaves and Significance of Hierarchical Structure for Superhydrophobicity and Low Adhesion. *Soft Matter* **2009**, *5*, 1386−1393.

(2) Langmuir, I. Overturning and Anchoring of Monolayers. *Science* **1938**, *87*, 493−500.

(3) Meyer, E. E.; Rosenberg, K. J.; Israelachvili, J. Recent Progress in Understanding Hydrophobic Interactions. *Proc. Natl. Acad. Sci. U. S. A.* **2006**, *103*, 15739−15746.

(4) Briscoe, W. H.; Klein, J. Friction and Adhesion Hysteresis between Surfactant Monolayers in Water. *J. Adhes.* **2007**, *83*, 705−722.

(5) Pesika, N. S.; Zeng, H.; Kristiansen, K.; Zhao, B.; Tian, Y.; Autumn, K.; Israelachvili, J. Gecko Adhesion Pad: A Smart Surface? *J. Phys.: Condens. Matter* **2009**, *21*, 464132.

(6) Tadmor, R.; Bahadur, P.; Leh, A.; Hartmann, E. N.; Jaini, R.; Dang, L. Measurement of Lateral Adhesion Forces at the Interface between a Liquid Drop and a Substrate. *Phys. Rev. Lett.* **2009**, *103*, 266101.

(7) Tadmor, R. Approaches in Wetting Phenomena. *Soft Matter* **2011**, *7*, 1577−1580.

(8) Leh, A.; Hartmann, E. N.; Fan, J.; Bahadur, P.; Tadmor, R.; Zhao, Y. On the Role of the Three-Phase Contact Line in Surface Deformation. *Langmuir* **2012**, *28*, 5795−5801.

(9) Shahsavan, H.; Arunbabu, D.; Zhao, B. Biomimetic Modification of Polymeric Surfaces: A Promising Pathway for Tuning of Wetting and Adhesion. *Macromol. Mater. Eng.* **2012**, *297*, 743−760.

(10) Tadmor, R. Line Energy and the Relation between Advancing, Receding, and Young Contact Angles. *Langmuir* **2004**, *20*, 7659−7664.

(11) Israelachvili, J. *Intermolecular and Surface Forces*, 2nd ed.; Academic Press: London, 1991.

(12) Chen, Y. L.; Helm, C. A.; Israelachvili, J. N. Molecular Mechanisms Associated with Adhesion and Contact Angle Hysteresis of Monolayer Surfaces. *J. Phys. Chem. C* **1991**, *95*, 10736−10747.

(13) Chen, Y.-L.; Israelachvili, J. N. Effects of Amblent Conditions on Adsorbed Surfactant and Polymer Monolayers. *J. Phys. Chem.* **1992**, *96*, 7752−7760.

(14) Chen, Y. L. E.; Gee, M. L.; Helm, C. A.; Israelachvili, J. N.; McGuiggan, P. M. Effects of Humidity on the Structure and Adhesion of Amphiphilic Monolayers on Mica. *J. Phys. Chem.* **1989**, *93*, 7051−7059.

(15) Min, Y.; Akbulut, M.; Prud'homme, R. K.; Golan, Y.; Israelachvili, J. Frictional Properties of Surfactant-Coated Rod-Shaped Nanoparticles in Dry and Humid Dodecane. *J. Phys. Chem. B* **2008**, *112*, 14395−14401.

(16) Min, Y.; Akbulut, M.; Kristiansen, K.; Golan, Y.; Israelachvili, J. The Role of Interparticle and External Forces in Nanoparticle Assembly. *Nat. Mater.* **2008**, *7*, 527−538.

(17) Belman, N.; Israelachvili, J. N.; Li, Y.; Safinya, C. R.; Ezersky, V.; Rabkin, A.; Sima, O.; Golan, Y. Hierarchical Superstructure of Alkylamine-Coated ZnS Nanoparticle Assemblies. *Phys. Chem. Chem. Phys.* **2011**, *13*, 4974−4979.

(18) McGuiness, C. L.; Diehl, G. A.; Blasini, D.; Smilgies, D.-M.; Zhu, M.; Samarth, N.; Weidner, T.; Ballav, N.; Zharnikov, M.; Allara, D. L. Molecular Self-Assembly at Bare Semiconductor Surfaces: Cooperative Substrate−Molecule Effects in Octadecanethiolate Monolayer Assemblies on GaAs(111), (110), and (100). *ACS Nano* **2010**, *4*, 3447−3465.

(19) McGuiness, C. L.; Shaporenko, A.; Mars, C. K.; Uppili, S.; Zharnikov, M.; Allara, D. L. Molecular Self-Assembly at Bare Semiconductor Surfaces: Preparation and Characterization of Highly Organized Octadecanethiolate Monolayers on GaAs(001). *J. Am. Chem. Soc.* **2006**, *128*, 5231−5243.

(20) Lide, D. R. *CRC Handbook of Chemistry and Physics*, 84th ed.; CRC Press: Boca Raton, FL, 2003−2004; pp 6-3, 6-153.

(21) Hirota, Y. Effects of Dissolved Oxygen in De-ionized Water Treatment on Gaas Surface. *J. Appl. Phys.* **1994**, *75*, 1798−1803.

(22) Bewig, K. W.; Zisman, W. A. The Wetting of Gold and Platinum by Water. *J. Phys. Chem.* **1965**, *69*, 4238−4242.

(23) Peczonczyk, S. L.; Mukerjee, J.; Carim, A. I.; Maldonado, S. Wet Chemical Fucntionalization of III-V Semiconductor Surfaces: Alkylation of Gallium Arsenide and Gallium Nitride by a Grignard Reaction Sequence. *Langmuir* **2012**, *28*, 4672−4682.

(24) Aveyard, R.; Haydon, D. A. *An Introduction to the Principles of Surface Chemistry*; Cambridge University Press: London, 1973; p 70.

(25) Davies, J. T.; Rideal, E. K. *Interfacial Phenomena*; Academic Press: New York, 1963; p 17.

(26) Lopes-Costa, T.; Gamez, F.; Lago, S.; Pedrosa, J. M. Adsorption of DNA to Octadecylamine Monolayers at the Air-Water Interface. *J. Colloid Interface Sci.* **2011**, *354*, 733−738.

(27) Lam, C. N. C.; Wu, R.; Li, D.; Hair, M. L.; Neumann, A. W. Study of the Advancing and Receding Contact Angles: Liquid Sorption As a Cause of Contact Angle Hysteresis. *Adv. Colloid Interface Sci.* **2002**, *96*, 169−191.

(28) Strobel, M.; Lyons, C. S. An Essay on Contact Angle Measurements. *Plasma Process. Polym.* **2011**, *8*, 8−13.

(29) Belman, N.; Israelachvili, J. N.; Li, Y.; Safinya, C. R.; Bernstein, J.; Golan, Y. The Temperature-Dependent Structure of Alkylamines and Their Corresponding Alkylamine-Alkylcarbamates. *J. Am. Chem. Soc.* **2009**, *131*, 9107−9113.

(30) Belman, N.; Israelachvili, J. N.; Li, Y.; Safinya, C. R.; Bernstein, J.; Golan, Y. Reaction of Alkylamine Surfactants with Carbon Dioxide: Relevance to Nanocrystal Synthesis. *Nano Lett.* **2009**, *9*, 2088−2093.

(31) Flores, A.; Ize, P.; Ramos, S.; Castillo, R. The Dioctadecylamine Monolayer: Textures, Phase Transitions, and Dendritic Growth. *J. Chem. Phys.* **2003**, *119*, 5644−5653.

(32) Gutierrez-Campos, A.; Diaz-Leines, G.; Castillo, R. Domain Growth, Pattern Formation, and Morphology Transitions in Langmuir Monolayers. A New Growth Instability. *J. Phys. Chem. B* **2010**, *114*, 5034−5046.

(33) Donaldson, S. H.; Lee, C. T.; Chmelka, B. F.; Israelachvili, J. N. General Hydrophobic Interaction Potential for Surfactant/Lipid Bilayers from Direct Force Measurements between Light-Modulated Bilayers. *Proc. Natl. Acad. Sci. U. S. A.* **2011**, *108*, 15699−15704.